K-shell Compton scattering at high photon energy

Viorica Florescu*
Department of Physics and Centre for Advanced Quantum Physics, University of Bucharest, MG-11, Bucharest-Măgurele 077125, Romania

R. H. Pratt
Department of Physics and Astronomy, University of Pittsburgh, Pittsburgh, Pennsylvania 15260, USA
(Received 2 July 2009; published 29 September 2009)

We examine very high energy Compton scattering on bound electrons, comparing cross sections obtained using relativistic impulse approximation (RIA) to the extreme relativistic (ER) limit of the exact Coulomb (EC) results for the 1*s* electron. For this purpose, in the case of an initial bound *s* state, we establish analytic expressions, valid within RIA, for the triply differential cross section (TDCS), corresponding to the detection of photons and electrons in coincidence, and for the ER limit of TDCS and of photon double-differential cross section (DDCS). We find that the RIA-ER expression for DDCS is the product of a simple factor, depending only on the ratio of initial and final photon frequencies, and a function of a single kinematic variable. Since the same structure is displayed by the EC-ER cross section, we present a compact representation of the ER results, in which the main differences between RIA-ER and EC-ER are displayed as a shift of the peak position of the frequency distribution and an asymmetry about that position. The comparison shows to what extent RIA, which becomes exact for vanishing nuclear charge *Z*, remains a good approximation for low and medium values of *Z* in the peak region of high-energy Compton scattering.

DOI: 10.1103/PhysRevA.80.033421 PACS number(s): 32.80.Aa

I. INTRODUCTION

In this paper, we study the *relativistic high-energy regime* of Compton scattering on bound electrons, comparing results from more approximate approaches to exact results in the high-energy limit. An overview of the theories used in Compton scattering from bound electrons at intermediate energies can be found in Ref. [1]. The most precise calculations [2] of Compton scattering on atoms are based on a numerical evaluation [3] of the second-order *S* matrix of quantum electrodynamics describing the process. The independent-particle approximation (IPA) is used for the electrons bound by a fixed nucleus. Based on this, doubly differential cross sections (DDCSs) are available for several elements at incident photon energies up to several hundred keV; the calculation was extended [4] to the triply differential cross sections (TDCSs), for which predictions were given for subshells. However, the case in which the photon energies are much larger than the electron rest mass energy is not accessible to these existing realistic calculations. The highest photon energy at which the *S*-matrix code has been used is 900 keV [5]. With increasing energy, there are difficulties connected with the poor convergence of the partial-wave series and multipolar expansion used in the numerical evaluation of the amplitude of the process. Having in mind these difficulties, an analytic expression for the extreme relativistic (ER) limit of the exact Coulomb (EC) matrix element of inelastic scattering by *K*-shell electrons was derived [6] and numerical calculations based on it were performed for both DDCS [6] and TDCS [7]. As we shall see in Sec. II, where the ER regime is defined in detail, this approach assumed that both the incident and the scattered photon frequencies ω_1 and ω_2 and the ejected electron momentum are extremely large, with a finite ratio ω_2/ω_1, and that the momentum transfer to the nucleus is finite. Up to now, these EC-ER results have not been compared to any other predictions. One of the purposes of our paper is to make such a comparison. The only somewhat reliable existing approximation at these energies appears to be the impulse approximation (IA), in its relativistic version (RIA), and we will compare EC-ER to RIA-ER.

IA is the most used approximation for Compton scattering on various targets. Introduced a long time ago, its nonrelativistic version was analyzed by Eisenberger and Platzman [8]; RIA was obtained by Ribberfors [9]. IA is argued, at least in the nonrelativistic case, to be valid for photon momentum transfer larger (or much larger) than the average momentum of the initially bound electron. The validity of impulse approximation has been the subject of recent studies [10], but only considering energies well below the electron rest mass energy. In view of the interest in using Compton scattering experiments to study atomic electron charge density, the relation of relativistic DDCS to the relativistic Compton profile (CP) was carefully investigated by Ribberfors [9], going beyond the first study of Eisenberg and Reed [11] who focused on the particular case of the 180° photon scattering angle and made further approximations.

The quantitative study we present later in our paper refers to the simple case of scattering from the 1*s* electron bound in a hydrogenlike atom. In order to confront predictions coming from EC-ER and RIA, we have found it is necessary to derive an ER limit of RIA. Because the further energy dependence of DDCS in RIA for $\omega_1, \omega_2 \gg 1$ (photon energies much larger than the electron rest mass energy), beyond the $1/\omega_1$ decrease predicted by ER, persists for photon energies of tens of MeV, we will only compare the ER case, for which

*flor@barutu.fizica.unibuc.ro

EC-ER results are available. One of our main findings is a useful way to compare the two sets of predictions, RIA-ER and EC-ER, by using appropriate variables that make clear the similarities and differences.

In discussing the behavior of the cross sections in the high-energy regime, we find it helpful to start from the behavior of Compton scattering on free electrons. For free electrons, both TDCS, describing the photon distribution in frequencies and angles in coincidence with the final electron direction, as well as DDCS for the scattered photon, obtained by integrating over final electron directions, are characterized by δ functions (two δ functions for TDCS and one δ function for DDCS). Only the singly differential cross section (the Klein-Nishina formula), obtained by integrating over either the direction or the frequency of the scattered photon, is finite. The presence of a potential in which the electrons move makes all the cross sections finite, peaked instead of δ function in character, affecting the position of their maxima and determining their widths. In the case of the point Coulomb potential of a fixed nucleus with charge Z, the transition from the initial free electron ($Z=0$) to the initial bound-electron cases can be followed in the Z dependence of the cross sections. However, in contrast with the nonrelativistic (NR) case, in the relativistic case an exact closed-form expression for the Coulomb Compton scattering amplitude is not available.

In IA, a bound electron is treated as a distribution of free electrons having the momentum distribution of the electron in the bound state. In the Coulomb case, this introduces the Z dependence of the cross sections. Being based on the free-electron Compton cross section, IA is unable to describe (i) the soft-photon limit ($\omega_2 \to 0$) behavior of the true cross sections, which display an infrared divergence, and (ii) the existence of resonances, which are present for any atomic states, except the ground state. Since it ignores the Coulomb effects in the propagator and in the final electron state, RIA accuracy may be expected to diminish with increasing αZ (α the fine-structure constant), but unlike in the nonrelativistic case, the error will still be present in the ER limit, of some significance for high Z. We may expect this effect to be less important than in the case of photoeffect, a process which requires the initial electron to be bound, as a free electron cannot absorb a photon, while Compton scattering occurs for the free-electron case, and the effects of binding diminish at high energies.

The paper is organized as follows. In Sec. II, we give our notations and define the relevant cross sections. In particular, we relate the usual TDCS to a cross section describing the distribution of the magnitude of the total momentum transfer, its azimuthal angle, and the scattered photon frequency and direction. At the end of the section, we give the conditions that define the ER regime.

Section III is devoted to a brief review of the free-electron case. The most differential cross section for an initial electron in motion is needed for RIA, while other cross sections, for an initial electron at rest, are useful for a qualitative understanding of the high-energy behavior of the cross sections.

In Sec. IV, we present the basic equations of RIA, particularly the expression of TDCS, not obtained in [9]. Revisiting RIA also gives us the opportunity to establish two new formulas, one for TDCS and the other for DDCS, describing the extreme relativistic limit of these RIA cross sections, denoted as RIA-ER. The decrease as $1/\omega_1$ of DDCS, known from the ER-EC case, appears explicitly. Apart from it, only the frequency ratio appears, in a simple factor F, given by Eq. (72), multiplying a function of a specific variable $\tilde{\Delta}^{\mathrm{ER}}_{\mathrm{min}}$ [see Eq. (63)]. At the end of the section, we refer to the particular case of scattering from a Coulomb K-shell electron. When, in Sec. V, we briefly describe the EC-ER results for this case, we notice a similar structure with that in RIA-ER, with the same factor F, now multiplied by a function of a variable specific to the EC-ER results. For our subsequent discussion, we reproduce from [6] simple analytic results for TDCS and DDCS, valid for $(\alpha Z)^2 \ll 1$. In Sec. VI, we relate the variables that are specific to DDCS in the two approaches and we decide that a convenient variable is $\tilde{\Delta}^{\mathrm{ER}}_{\mathrm{min}}$. For small αZ, we compare the specific analytic results which can be obtained in the two approaches.

Section VII exploits the features of the analytic results found in this work. The use of the variable $\tilde{\Delta}^{\mathrm{ER}}_{\mathrm{min}}$ in Figs. 1–3 makes transparent the comparison of RIA-ER and EC-ER results for DDCS. In the peak region, for which $\tilde{\Delta}^{\mathrm{ER}}_{\mathrm{min}}/\alpha Z \leq 1$ (momentum transferred to the nucleus close to the average momentum of the K-shell electron), the comparison illustrates both the validity of the ER limit of RIA in the small αZ regime (relative errors less than 4% for $Z<29$ for DDCS) and the Z-dependent effects at high Z (10% for $Z=82$). Figure 4 is devoted to a comparison of DDCS predicted by RIA-ER to the Compton profile approximation. In Fig. 5, TDCS are compared in the ER regime. A way to combine RIA and EC-ER results, which could be useful in the high-energy regime, is suggested. The Appendix gives some details of nonrelativistic impulse approximation (NRIA), including TDCS, and some equations needed for the ER limit of RIA.

II. GENERAL NOTATIONS AND PARAMETERS: TRIPLY AND DOUBLY DIFFERENTIAL CROSS SECTIONS

In the following, we use units with $c=m_e=\hbar=4\pi\epsilon_0=1$. We consider the scattering of photons of definite momentum $\boldsymbol{\kappa}_1$ on a bound electron of total energy E_0. In the units we use, the magnitude of $\boldsymbol{\kappa}_1$ coincides with the photon energy or with its frequency, already denoted by ω_1. The incident photon energy ω_1 will be taken, such as the atomic number Z, as a parameter specifying the initial conditions.

The scattered photon has a momentum $\boldsymbol{\kappa}_2$ (magnitude ω_2) and the ejected electron a momentum $\mathbf{p}$. The scattering angle of the photon is denoted by θ. The final electron energy and momentum are connected by $E=\sqrt{1+\mathbf{p}^2}$.

In this paper, we treat only the situation in which the polarization properties of the initial and final particles (electrons and photons) are not observed. In this situation, the most differential cross section $d^4\sigma$, specifying the observed $\boldsymbol{\kappa}_2$ and $\mathbf{p}$ for specified $\boldsymbol{\kappa}_1$, and initial energy E_0 of the bound electron being ejected, contains a δ function expressing energy conservation

$$d^4\sigma = \sigma_3 \delta(\omega_2 + E - \omega_1 - E_0) d\omega_2 d\Omega_2 dE d\Omega_e. \quad (1)$$

If the scattering takes place on an atomic bound s state, the function σ_3 depends only on the scalars $\boldsymbol{\kappa}_2 \cdot \boldsymbol{\kappa}_1$, $\mathbf{p} \cdot \boldsymbol{\kappa}_1$, and $\mathbf{p} \cdot \boldsymbol{\kappa}_2$ built from the three vectors $\boldsymbol{\kappa}_1, \boldsymbol{\kappa}_2$, and $\mathbf{p}$ (pseudoscalars do not appear due to the invariance under parity of the electron-photon interaction). In a system of reference with the $0z$ axis along the initial photon direction, i.e., along $\boldsymbol{\kappa}_1$, and otherwise arbitrary, the scattered photon direction is characterized by the polar angles θ, defined before, and by an azimuthal angle ϕ_γ and the electron direction by the polar angles denoted by θ_e and ϕ_e. The angular variables associated with the three scalars are θ, θ_e, and $\phi_e - \phi_\gamma$,

$$\boldsymbol{\kappa}_2 \cdot \boldsymbol{\kappa}_1 = \omega_2 \omega_1 \cos\theta, \quad \mathbf{p} \cdot \boldsymbol{\kappa}_1 = p\omega_1 \cos\theta_e, \quad (2)$$

$$\mathbf{p} \cdot \boldsymbol{\kappa}_2 = p\omega_2 [\cos\theta \cos\theta_e + \sin\theta \sin\theta_e \cos(\phi_e - \phi_\gamma)]. \quad (3)$$

The dependence of the cross section on only the three angles mentioned above is due to the isotropy of the space expressed here in an independence of the results on the position of the plane containing the incident and the scattered photon momenta.

The momentum transfer of the photon in scattering is

$$\mathbf{K} = \boldsymbol{\kappa}_1 - \boldsymbol{\kappa}_2. \quad (4)$$

A basic quantity is *the total momentum transfer* to the nucleus

$$\boldsymbol{\Delta} = \boldsymbol{\kappa}_1 - \boldsymbol{\kappa}_2 - \mathbf{p} = \mathbf{K} - \mathbf{p}. \quad (5)$$

These two vectors $\mathbf{K}$ and $\boldsymbol{\Delta}$ will be used further.

Integration over the final electron energy, determined by the δ function, leads to a distribution in the electron direction and the photon frequency and direction, expressed as the TDCS cross section

$$\sigma_3 \equiv \frac{d^3\sigma}{d\omega_2 d\Omega_2 d\Omega_e}, \quad (6)$$

where σ_3 depends on four variables: the three angles θ, θ_e, and $\phi_e - \phi_\gamma$ mentioned before and the scattered photon frequency.

If only the scattered photon frequency and direction are observed, one is interested in the DDCS cross section

$$\sigma_2 \equiv \frac{d^2\sigma}{d\omega_2 d\Omega_2} = \int_{\theta_e, \phi_e} \sigma_3 d\Omega_e. \quad (7)$$

The integration over θ_e and ϕ_e is in fact an integration over θ_e and $\phi_e - \phi_\gamma$ and it leads to a cross section σ_2 depending only on two variables, the scattered photon frequency and the scattering angle θ, in agreement with the symmetry noticed before.

In the case of an initially bound electron, where there is no δ function in DDCS, ω_2 and θ are two independent variables. We shall use in the following two alternative independent variables directly related to ω_2 and θ:

$$\eta \equiv \frac{\omega_2}{\omega_1}, \quad \xi \equiv \omega_1(1 - \cos\theta), \quad (8)$$

in terms of which DDCS may also be written. In these two sets of variables, the square of the photon momentum transfer is expressed as

$$K^2 = \omega_1^2 + \omega_2^2 - 2\omega_1\omega_2 \cos\theta = \omega_1^2(1-\eta)^2 + 2\omega_1\xi\eta. \quad (9)$$

Besides the variables η and ξ (or ω_2 and θ) defined above, the TDCS depends also on the angles of the electron direction, specified above in a system of reference $0xyz$ with the $0z$ axis along the fixed incident photon momentum. With respect to an alternative reference system $0XYZ$ with the $0Z$ axis along the photon momentum transfer $\mathbf{K}$, the vector $\mathbf{p}$ will have polar angles denoted by (β, ϕ). We do not need to specify the choice of the other axes in either case. This second pair of angles is more convenient for expressing the analytic results obtained in our work. The dependence of $\cos\beta$ on the angles defined previously is

$$K\cos\beta = \omega_1 \cos\theta_e - \omega_2[\cos\theta_e \cos\theta + \sin\theta_e \sin\theta \cos(\phi_e - \phi_\gamma)]. \quad (10)$$

The angle β between the ejected electron momentum $\mathbf{p}$ and the photon momentum transfer $\mathbf{K}$ will play an important role in the following.

In the ER calculation in [6], the scattering was characterized by $\boldsymbol{\kappa}_1, \boldsymbol{\kappa}_2$ and $\boldsymbol{\Delta}$ instead of $\boldsymbol{\kappa}_1, \boldsymbol{\kappa}_2$ and $\mathbf{p}$. Having in mind the comparison, we shall make between RIA-ER and EC-ER results, we find it convenient to replace the angular variable β of the electron by the magnitude Δ of the total momentum transfer, as done in [6]. As

$$\Delta^2 = p^2 + K^2 - 2pK\cos\beta \quad (11)$$

and the magnitude of $\mathbf{p}$ is given by energy conservation [as implied by Eq. (1)], the relation between Δ and β is simple and direct.

Using Δ instead of β, we define the multiply differential cross section

$$\Sigma_3 \equiv \frac{d^3\sigma_{\mathrm{ER}}}{d\omega_2 d\Omega_2 d\Delta d\Phi}, \quad (12)$$

which represents the distribution over the scattered photon frequency and scattering angle and over the values taken by the magnitude Δ and the azimuthal angle Φ of the total momentum transfer in the system of reference $0XYZ$. In fact, as according to Eq. (5), $\mathbf{K} = \mathbf{p} + \boldsymbol{\Delta}$, the three vectors are coplanar, and as $\mathbf{K}$ is taken as the $0Z$ axis, the two azimuthal angles Φ of $\boldsymbol{\Delta}$ and ϕ of $\mathbf{p}$ differ by π and then $d\Phi = d\phi$. The connection of Σ_3 with the usual triply differential cross section σ_3 in Eq. (6) is obtained from Eq. (11), which gives

$$\Delta d\Delta = pK \sin\beta d\beta. \quad (13)$$

In this way, we have $d\Delta d\Phi = \frac{pK}{\Delta} d\Omega_e$ and

$$\sigma_3 = \frac{pK}{\Delta} \Sigma_3. \quad (14)$$

Now we describe the ER regime. This regime involves a limiting situation in which the photons and the ejected electrons have very large energies, but the ratio $\omega_2/\omega_1=\eta$ is finite. Related situations are met in the high-energy limit of K-shell photoeffect [12] and of Rayleigh scattering [13], as in all cases the incident photon frequency ω_1 is supposed to be very large. For Rayleigh and Compton scatterings, a scattered photon of frequency ω_2 is present (in the Rayleigh case $\omega_2=\omega_1$) and this frequency is also very large.

Precisely, the ER regime is defined by the conditions

$$\omega_1 \to \infty, \quad \epsilon' < \eta < 1-\epsilon, \quad \Delta = \text{finite}, \tag{15}$$

where Δ is the total momentum transfer defined in Eq. (5) and η is defined in Eq. (8); ϵ' and ϵ are positive, sufficiently small fixed quantities, independent of ω_1. The second condition implies both $\omega_2 \to \infty$ and $p \to \infty$. Then, as we shall argue in the following, the third condition implies finite values for ξ and $\omega_1 \sin \beta/2$, i.e., a behavior such as $1/\sqrt{\omega_1}$ for the angle θ and as $1/\omega_1$ for the polar angle of the final electron.

Now we give some explanations of the conditions we have listed and the justification of their implications. In [6], where the case of a initial K-shell electron of a hydrogenlike atom was considered, it was noted that the amplitude of Compton scattering goes to zero much faster for very large values of Δ than for finite or zero values due to a rapidly oscillating factor in the integral which determines this amplitude. This is why only this latter domain for Δ is investigated in the ER limit. This argument is more general, valid for other bound states and for other than Coulomb potentials. For the ratio η, one distinguishes three regions. Two of them, the soft-photon end (η near 0) and the tip of the spectrum (η close to 1), require a separate treatment and we will not treat them in our discussion. By excluding the region near 0 for η, we have $\omega_2 \to \infty$, and by excluding the tip of the spectrum, we deal with very large values of the electron momentum $p \approx \omega_1(1-\eta) \to \infty$. The third region, including the position of the Compton line for scattering from free electrons and the region of the Compton peak in scattering from bound electrons, as characterized by Eq. (14) of [6], corresponds to the second condition in Eq. (15).

In order to see the implications of Eq. (15), one has to analyze the total momentum transfer Δ of Eq. (11) for $\omega_1 \to \infty$. We use energy conservation, as implied by Eq. (1) and the expression (9) for K. As $\eta \neq 1$, from energy conservation, one has

$$p = \omega_1(1-\eta) + E_0 + O\left(\frac{1}{\omega_1}\right). \tag{16}$$

This explains how p goes to ∞ as ω_1.

If now we write for the total momentum transfer magnitude

$$\Delta^2 = (p-K)^2 + 2pK(1-\cos\beta)^2, \tag{17}$$

for Δ to be finite, then both terms have to be finite. From the first term, we deduce that K has to go to ∞ the same way as p does, which is possible, as Eq. (9) and (16) show, *only if* the photon scattering angle θ goes to 0 as $1/\sqrt{\omega_1}$, leading to

$$\xi = \text{finite}. \tag{18}$$

This is the content of Eq. (24) of [6], but now we have obtained it for a more general potential. Using it and the expression (9) of K^2, we get as $\omega_1 \to \infty$,

$$K = \omega_1(1-\eta) + \frac{\xi\eta}{1-\eta} + O\left(\frac{1}{\omega_1}\right). \tag{19}$$

Now, knowing the behavior of p and K, the requirement for a finite Δ leads to the conclusion that a new quantity has to be finite, namely,

$$\zeta \equiv \omega_1 \sin\frac{\beta}{2} = \text{finite}. \tag{20}$$

This shows that a finite momentum transfer implies that the scattering angle β of the electron momentum goes to 0 as $1/\omega_1$, which is faster than the decrease as $1/\sqrt{\omega_1}$ of θ required by Eq. (18). The dominant cross sections are obtained at these angles.

Finally, using all the previous information, we get, for $\omega_1 \to \infty$,

$$\Delta^2 \to q^2 + 4\xi^2(1-\eta)^2 \equiv (\Delta^{\mathrm{ER}})^2, \quad q \equiv \frac{\xi\eta}{1-\eta} - E_0. \tag{21}$$

One sees that the values taken by Δ^{ER} are restricted by

$$\Delta^{\mathrm{ER}} \geq |q|, \tag{22}$$

a condition that reduces to Eq. (29) of [6] for the K shell in the Coulomb case. Thus the modulus of q has the meaning of the minimum value for the magnitude of the total momentum transfer allowed in the ER regime. This variable Δ^{ER} will be used in presenting results for the triply differential cross section Σ_3 defined in Eq. (12).

III. SCATTERING ON FREE ELECTRONS

The equations corresponding to scattering from an initial free electron in motion are directly used in RIA for deriving the expression of TDCS, which was not written explicitly before, although predictions for it appear in [4]. The case of the initial free electron at rest helps to understand the behavior in the ER limit of the bound case results, as has been calculated in the Coulomb potential [6].

In Compton scattering from a free electron of momentum $\mathbf{p}_0$, not necessarily at rest, both energy and momentum are conserved

$$\omega_1 + E(p_0) = \omega_2 + E(p), \quad \boldsymbol{\kappa}_1 + \mathbf{p}_0 = \boldsymbol{\kappa}_2 + \mathbf{p}, \tag{23}$$

employing a notation we shall use systematically hereafter, for any momentum,

$$E(p) \equiv \sqrt{1+p^2}. \tag{24}$$

The most differential cross section $d^4\sigma_{\mathrm{KN}}$ for Compton scattering *from a moving free electron*, summed over the final electron spin and scattered photon polarization and averaged over the corresponding observables of the initial electron and photon, is

$$d^4\sigma_{\mathrm{KN}} = r_0^2 \frac{X(R_1,R_2)}{2R_1E(p)\omega_2}\delta(\mathbf{p}+\boldsymbol{\kappa}_2-\boldsymbol{\kappa}_1-\mathbf{p}_0) \times \delta[E(p)+\omega_2-E(p_0)-\omega_1]d\boldsymbol{\kappa}_2 d\mathbf{p}. \quad (25)$$

This expression can be extracted from Jauch and Rohrlich [14], Eqs. (11.9) and (11.14); we use slightly different notations, namely,

$$R_j = E(p_0)\omega_j - \mathbf{p}_0\cdot\boldsymbol{\kappa}_j, \quad j=1,2, \quad (26)$$

$$X(R_1,R_2) \equiv \frac{R_1}{R_2}+\frac{R_2}{R_1}+2\left(\frac{1}{R_1}-\frac{1}{R_2}\right)+\left(\frac{1}{R_1}-\frac{1}{R_2}\right)^2. \quad (27)$$

The R_j satisfy the simple relation $R_2=R_1-\omega_1\omega_2\,(1-\cos\theta)$. In Sec. IV, the expression (25) will be used to obtain TDCS and DDCS in RIA.

Momentum conservation makes the vector $\boldsymbol{\Delta}$ as defined in Eq. (5) equal, up to a sign, to the initial electron momentum $\mathbf{p}_0$. The two δ functions (the first three-dimensional) in Eq. (25) determine four of the six quantities characterizing the cross sections. For instance, if one fixes the direction of the scattered photon, all the other variables are determined.

In the following equations of this section, we shall assume that the initial electron is at rest, $\mathbf{p_0}=\mathbf{0}$. This introduces a symmetry to the problem, making the cross section independent on the position of the plane containing the photon momenta; this plane contains also the final electron momentum and this explains why the azimuthal angles of the final particles, which differ by π, do not appear in the factor that multiplies the δ functions in Eq. (25). So the only variable of the cross sections is the photon scattering angle θ, the other quantities being determined by the conservation laws expressed by the δ functions, as follows. The scattered photon frequency given by the well-known Compton formula,

$$\omega_2 = \frac{\omega_1}{1+\omega_1(1-\cos\theta)} \equiv \omega^{\mathrm{Co}}, \quad (28)$$

reads simply in the variables (8),

$$\eta = \frac{1}{1+\xi}. \quad (29)$$

The final electron momentum has magnitude

$$p^{\mathrm{free}} = \sqrt{(\omega_1-\omega_2)(\omega_1-\omega_2+2)} = \omega_1(1-\eta)\sqrt{1+\frac{2}{(1-\eta)\omega_1}} = \omega_1\frac{\xi}{1+\xi}\sqrt{1+\frac{2(1+\xi)}{\xi\omega_1}} \quad (30)$$

and its angle θ_e^{free} with the incident photon follows from

$$\cos\theta_e^{\mathrm{free}} = \frac{1-\eta}{p^{\mathrm{free}}}(1+\omega_1) = \frac{\xi(1+\omega_1)}{p^{\mathrm{free}}(1+\xi)}. \quad (31)$$

Of course, as $\boldsymbol{\kappa}_1$ is the sum of $\mathbf{p}$ and $\boldsymbol{\kappa}_2$, in any frame of reference with the $0z$ axis along $\boldsymbol{\kappa}_1$, the azimuthal angles of $\mathbf{p}$ and of $\boldsymbol{\kappa}_2$ differ by π. For our further use, we have expressed p^{free} and $\cos\theta_e^{\mathrm{free}}$ in terms of either η or alternatively ξ, together with ω_1. Finally, the expression (27) for the function X reduces to

$$X_0 = \eta+\frac{1}{\eta}+\frac{2}{\omega_1}\left(1-\frac{1}{\eta}\right)+\frac{1}{\omega_1^2}\left(1-\frac{1}{\eta}\right)^2 = \frac{1}{1+\xi}+1+\xi-2\frac{\xi}{\omega_1}+\frac{\xi^2}{\omega_1^2}. \quad (32)$$

In order to obtain TDCS, the integral over the final electron energy is performed using the second δ function in Eq. (25). The first δ function in Eq. (25) remains, but with the magnitude of the vector $\mathbf{p}$ now determined by energy conservation, as given in Eq. (30).

Integration over the electron direction leads to the DDCS. This cross section can be obtained more easily directly from Eq. (25), integrating over the final electron momentum. The result

$$d^2\sigma_{\mathrm{KN}} = r_0^2\frac{X_0}{2}\frac{\delta(\omega_2-\omega^{\mathrm{Co}})}{[1+\omega_1(1-\cos\theta)]^2}d\omega_2 d\Omega_2, \quad (33)$$

in which ω^{Co} is the Compton frequency in Eq. (28), still contains a δ function. Finally, integration over the final photon frequency leads to the Klein-Nishina formula, giving the distribution in photon directions. If we integrate over the azimuthal angle ϕ_γ of the scattered photon, on which the cross section does not depend, we get

$$\frac{d\sigma_{\mathrm{KN}}}{d\Omega_2} = \pi r_0^2\frac{X_0}{[1+\omega_1(1-\cos\theta)]^2}\sin\theta d\theta = \pi r_0^2\frac{X_0}{\omega_1(1+\xi)^2}d\xi, \quad (34)$$

where the final form Eq. (32) for X_0 is used, in which, according to Eq. (8), ξ is a function of ω_1 and θ. As is well known, this can be alternatively written as a distribution in the final frequency, using Eq. (29),

$$d\sigma = \frac{\pi r_0^2}{\omega_1^2}X_0 d\omega_2. \quad (35)$$

For further reference, we give the ER behavior of the final electron-momentum magnitude and scattering angle and for the quantity X_0,

$$p^{\mathrm{free}} = \omega_1(1-\eta)+1+O(1/\omega_1),$$

$$\cos\theta_e^{\mathrm{free}} = 1-\frac{\eta}{\omega_1}+O(1/\omega_1^2), \quad X_0^{\mathrm{ER}} = \eta+\frac{1}{\eta}. \quad (36)$$

IV. TDCS AND DDCS IN IMPULSE APPROXIMATION

In this section, we describe RIA in some detail, obtaining DDCS via TDCS. This is an alternative procedure to that of Ribberfors [9], who studied DDCS only and did the integration over the final electron momentum before that over the initial electron momentum; as a consequence, TDCS was not obtained in his calculation. Apart from the meaning of the variables involved, the main steps implied by the calculations are similar as the interchanges $\mathbf{p}\leftrightarrow-\mathbf{p}_0$ and $E\leftrightarrow-E_0$ reduce one case to the other one.

The starting point for the IA is the most differential relativistic cross section discussed in the previous section, given by Eq. (25). It corresponds to colliding beams, so it was obtained by dividing the transition rate by the relative flux I of incident photon and electron, $I=R_1/[V\omega_1 E(p_0)]$ [see Eq. (8-47) of [14], with V, the space volume, going to ∞, but not present in the final equations]. For the impulse approximation, where one deals with a distribution of initial momenta, this cross section is not useful [9,11]: as in the bound-state case, we need the ratio of the transition rate divided by the incident photon flux $1/V$ only. This is the same as the flux I taken for the electron at rest [15]. This leads to a cross section $\widehat{d^4\sigma}$ that we mark by a $\widehat{\ }$ in order to distinguish it from the cross section $d^4\sigma_{\mathrm{KN}}$ in Eq. (25) or the RIA cross section $d^4\sigma_{\mathrm{RIA}}$ which we will next obtain by averaging over the initial electron-momentum distribution

$$\widehat{d^4\sigma} = r_0^2 \frac{m_e^2}{2E(p_0)E(p)\omega_1\omega_2} X(R_1,R_2) \times \delta(\mathbf{p}+\boldsymbol{\kappa}_2-\boldsymbol{\kappa}_1-\mathbf{p}_0)\delta[E(p)+\omega_2-E(p_0)-\omega_1]d\boldsymbol{\kappa}_2 d\mathbf{p}. \tag{37}$$

According to the main idea of IA, Compton scattering on a bound electron is viewed as inelastic photon scattering on an ensemble of free electrons having the momentum distribution of the bound electron. The relevant relativistic momentum distribution is

$$\rho(\mathbf{p}_0) = \chi^\dagger(\mathbf{p}_0)\chi(\mathbf{p}_0), \tag{38}$$

where the bispinor χ is the Fourier transform of the bound-state bispinor. Then, the relativistic Compton scattering cross section from a bound electron in this model is

$$d^4\sigma_{\mathrm{RIA}} = \int_{\mathbf{p}_0} \widehat{d^4\sigma}\rho(\mathbf{p}_0)d\mathbf{p}_0, \tag{39}$$

with the differential cross section $\widehat{d^4\sigma}$ given by Eq. (37).

The momentum δ function in Eq. (37) allows the integral over $\mathbf{p}_0$ to be performed directly, leading to

$$d^4\sigma_{\mathrm{RIA}} = r_0^2 \frac{m_e^2}{2E(\Delta)E(p)\omega_1\omega_2} X(R_1,R_2)\Big|_{\mathbf{p}_0=\mathbf{p}-\mathbf{K}} \times \delta[E(p)+\omega_2-E(|\mathbf{p}-\mathbf{K}|)-\omega_1]\rho(\mathbf{p}-\mathbf{K})d\boldsymbol{\kappa}_2 d\mathbf{p}. \tag{40}$$

Note that the energy conservation δ function here differs from that of the physical case, Eq. (1), as $E(|\mathbf{p}-\mathbf{K}|)\neq E_0$. It follows, as we shall see in detail in the following, that the value attributed to the magnitude of the ejected momentum by the δ function is different from the magnitude of the physical momentum and the same will be true for the magnitude and direction of the total momentum transfer $\boldsymbol{\Delta}$ to the nucleus. Consequently, we shall use the notation $\tilde{p}$ for the magnitude of the electron momentum in RIA, $\tilde{\mathbf{p}}$ for the corresponding vector, and $\tilde{\boldsymbol{\Delta}}$ for the associated momentum transfer

$$\tilde{\boldsymbol{\Delta}} \equiv \boldsymbol{\kappa}_1 - \boldsymbol{\kappa}_2 - \tilde{\mathbf{p}}. \tag{41}$$

The cross section (40) and those following from it by integrating over quantities not observed have to be compared to the predictions coming from other approaches.

A. TDCS in RIA

In order to get the *triply differential cross section* with respect to the final photon energy and direction and final electron direction, we have to integrate over the magnitude of the final electron momentum. The δ function in Eq. (40) implies the equation

$$E(\tilde{p}) + \omega_2 - \omega_1 = E(\tilde{\Delta}). \tag{42}$$

This equation can be written in different forms. From its square, we get the *implicit* form

$$\tilde{p}K\cos\beta = E(\tilde{p})(\omega_1-\omega_2) + \omega_1\omega_2(1-\cos\theta). \tag{43}$$

This shows that $\cos\beta>0$, i.e., the scattering angle of the ejected electron in IA cannot be larger than $\pi/2$ since the right-hand side is nonnegative, but we shall see in what follows that the restriction imposed on β is stronger. Of course, exact results do not have this restriction.

Our condition (43) resembles Eq. (16) of Ribberfors [9]. The difference in sign comes from the fact that the same letters E and β have different meanings in the relations we compare. As already mentioned, Ribberfors integrated first over the final electron momentum at fixed momentum of the incident electron. So, in Ribberfors case, E and β refer to the initial electron; in our case, they refer to the final electron. Given the role played by the two electron momenta in the energy and momentum conservation relations, it follows that the change from (E,β) to $(-E,\pi-\beta)$ will transform Ribberfors equation (16) in our Eq. (43), which is the case. Also, given the different meaning, Ribberfors equation allows his angle β to have any value.

From the condition (42), one derives a second-order equation for $\tilde{p}$,

$$[K^2\sin^2\beta - 2\omega_1\xi\eta]\tilde{p}^2 - 2\omega_1\xi\eta K\tilde{p}\cos\beta + \omega_1^2[\xi^2\eta^2-(1-\eta)^2] = 0, \tag{44}$$

or, alternatively, a second-order equation for the associated energy $\tilde{E}\equiv E(\tilde{p})$,

$$[K^2\sin^2\beta - 2\omega_1\xi\eta]\tilde{E}^2 + 2\xi\eta(1-\eta)\omega_1^2\tilde{E} + [\xi^2\eta^2\omega_1^2 + K^2\cos^2\beta] = 0. \tag{45}$$

Both equations are useful in finding the good solution of Eq. (42). Equation (45) has one positive solution only if

$$\beta \le \beta_{\max}, \quad \cos\beta_{\max} = (1-\eta)\frac{\omega_1}{K} < 1. \tag{46}$$

The corresponding solution for $\tilde{p}$ is

$$\tilde{p} = \frac{\xi\eta\omega_1}{2\omega_1\xi\eta - K^2\sin^2\beta}\left[K\cos\beta + \omega_1(1-\eta)\right.$$
$$\left.\times\left(1 + \frac{2}{\omega_1\xi\eta} - \frac{K^2\sin^2\beta}{\omega_1^2\xi^2\eta^2}\right)^{1/2}\right]. \quad (47)$$

The condition (46) shows that the angular range for the angle β allowed by RIA is narrower than in the NR case, where β is allowed to reach values up to $\pi/2$.

The derivative of $\tilde{p}$ with respect to β is positive; $\tilde{p}$ starts from a value denoted by $\tilde{p}_{\min}$ taken for $\beta=0$ and increases up to ∞, when the angle β reaches the value $\beta_{\max}$ defined in Eq. (46). The solution $\tilde{p}$ of Eq. (43), given by Eq. (47), represents a fictitious value attributed to the magnitude of the final electron momentum in the formalism of RIA. Note that *the value of* $\tilde{p}$ depends on both of the angles β and θ, which is not the case for the true outgoing momentum resulting from energy conservation [see Eq. (1)], depending only on the energies of the other particles. The corresponding result for $\tilde{p}$ in NRIA (nonrelativistic IA) is Eq. (A3).

The needed integration on the final electron energy $E(p)$ to obtain σ_3^{RIA} from $d^4\sigma_{\mathrm{RIA}}$ in Eq. (40) takes into account that Δ depends on p using the identity

$$\delta(E(p) + \omega_2 - E(\Delta) - \omega_1)$$
$$= \frac{E(\tilde{\Delta})E(\tilde{p})}{|(\omega_1-\omega_2)\tilde{p} - E(\tilde{p})K\cos\beta|}\delta(p-\tilde{p}). \quad (48)$$

The result is

$$\sigma_3^{\mathrm{RIA}} \equiv d^3\sigma_{\mathrm{RIA}}/d\omega_2 d\Omega_2 d\Omega_e$$
$$= r_0^2\frac{m_e^2}{2}\eta\frac{\tilde{p}^2 X(\tilde{R}_1,\tilde{R}_2)}{|(\omega_1-\omega_2)\tilde{p} - E(\tilde{p})K\cos\beta|}\rho(-\tilde{\mathbf{\Delta}}). \quad (49)$$

The expressions of $\tilde{R}_1$ and $\tilde{R}_2$ are obtained from those of R_1 and R_2 in Eq. (26) with $\mathbf{p}_0 = -\tilde{\mathbf{\Delta}}$, which leads to

$$\tilde{R}_1 = \omega_1 E(\tilde{\Delta}) + \tilde{\mathbf{\Delta}}\cdot\boldsymbol{\kappa}_1, \quad \tilde{R}_2 = \tilde{R}_1 - \omega_1\xi\eta. \quad (50)$$

Remember that $\tilde{p}$ depends on the angle β, being the solution of Eq. (43), explicitly written in Eq. (47).

Equation (49) is our result for TDCS in RIA. It is valid for any electron state if IPA is adopted. The atomic state on which the scattering takes place enters in the specification of the momentum density distribution ρ of its charge density. In the case of a bound s state, the TDCS depends on the electron direction through $\tilde{\Delta}$ and the scalar product $\tilde{\mathbf{\Delta}}\cdot\boldsymbol{\kappa}_1$. In a fixed system of reference $0xyz$ with the $0z$ axis along the incident photon direction, TDCS depends on the polar angle θ of the scattered photon, the polar angle θ_e of the electron, and on the difference between their azimuthal angles ϕ_e and ϕ_γ. The last variable is due to cos β with the expression (10).

B. DDCS in RIA

We describe briefly how the DDCS of Ribberfors emerges from the expression given above for TDCS. For this purpose, we calculate

$$\sigma_2^{\mathrm{RIA}} \equiv \frac{d^2\sigma_{\mathrm{RIA}}}{d\omega_2 d\Omega_2} = \int_{\tilde{\mathbf{p}}/\tilde{p}} \sigma_3^{\mathrm{RIA}} d\Omega_e, \quad (51)$$

i.e., we integrate over the final electron directions. The integration over the final electron azimuthal angle is always possible for a charge density with spherical symmetry and can be done easily. This calculation is elementary and formally identical to that Ribberfors performed for the integration on the azimuthal angle of the initial electron after the integration over the final electron momentum had been done. We describe briefly how the calculation proceeds in our case. In order to do the angular integration, one starts with a reference system $0xyz$ denoted as S_1, with the $0z$ axis along the incident photon momentum and the $0xz$ plane containing the scattered photon. Automatically this plane contains also the vector $\mathbf{K}$. Then one uses a second system of reference $0XYZ$, denoted by S_2, with the $0Z$ axis along $\mathbf{K}$ and with the same $0Y$ axis as S_1. These two systems are simply connected by a rotation around the common $0y$ axis [17]. In the system of reference S_2, the final electron momentum has β as the polar angle and an azimuthal angle denoted by Φ. Integration over θ_e and ϕ_e can be transformed in to an integration over β and Φ. This last angle will now appear in the scalar product $\tilde{\mathbf{\Delta}}\cdot\boldsymbol{\kappa}_1$ in Eq. (50). Then we make a change of variable, from the angle β to $\tilde{\Delta}$, using the definition (41),

$$\tilde{\Delta} = |\mathbf{K} - \tilde{\mathbf{p}}| = \sqrt{\tilde{p}^2 + K^2 - 2\tilde{p}K\cos\beta}, \quad (52)$$

in which $\tilde{p}$ satisfies Eq. (43). One sees that $\tilde{\Delta}$ depends on β directly and also indirectly via $\tilde{p}$. Taking this into account, one shows that the minimum value taken by $\tilde{\Delta}$ coincides with the quantity p appearing in Ribberfors' exact equation (16), which is an implicit expression for p. After this, the final analytic result for DDCS becomes identical to Ribberfors Eq. (39). We partially reproduce it here using nevertheless our notation for the integration variable and its limit

$$\sigma_2^{\mathrm{RIA}} = r_0^2\pi\frac{\eta}{K}\int_{\tilde{\Delta}_{\min}}^{\infty}\frac{\tilde{\Delta}}{E(\tilde{\Delta})}\rho(\tilde{\Delta})\bar{X}_{\mathrm{int}}(\omega_1,\xi,\eta;\tilde{\Delta})d\tilde{\Delta}. \quad (53)$$

The function $\bar{X}_{\mathrm{int}}$, in which we have specified all the variables, is that in Eq. (37) of Ribberfors, if the following correspondences between Ribberfors' notation and ours are observed,

$$\omega \to \omega_1, \quad \omega' \to \omega_2, \quad p \to \tilde{\Delta}, \quad \beta \to \pi - \beta. \quad (54)$$

We reproduce the expression of $\bar{X}_{\mathrm{int}}$ in the Appendix [Eqs. (A10)–(A13)].

The integration limit $\tilde{\Delta}_{\min}$, introduced in Eq. (53), is taken for $\beta=0$, so it is $\tilde{\Delta}_{\min} = |\tilde{p}_{\min} - K|$, with $\tilde{p}_{\min} = \tilde{p}(\beta=0)$ obtained from Eq. (47),

$$\tilde{\Delta}_{\min} = \frac{1}{2}\left|K - \omega_1(1-\eta)\left(1 + \frac{2}{\omega_1\xi\eta}\right)^{1/2}\right|. \quad (55)$$

We note that the value of $E(\tilde{\Delta}_{\min}) = \sqrt{1+\tilde{\Delta}_{\min}^2}$ that follows is in agreement with the expression given in Eq. (4) of [10].

In the *nonrelativistic regime*, $\omega_1 \ll 1$, the limit $\tilde{\Delta}_{\min}$ approaches the expression of p_z, with p_z defined in Eq. (A7) of the Appendix, if $|\omega_2 - \omega_1| \ll 2\omega_1\omega_2(1-\cos\theta)$; in particular, this happens near the Compton line (28). The relation between the relativistic integration limit used in evaluating DDCS based on Eq. (53) and the nonrelativistic integration limit and the dependence on Z due to the relativistic limit on the numerical results were recently investigated by LaJohn [18].

$\tilde{\Delta}_{\min}$ satisfies the equation

$$K\tilde{\Delta}_{\min} = \omega_1 |(1-\eta)E(\tilde{\Delta}_{\min}) - \xi\eta|, \tag{56}$$

identical with Ribberfors' equation (16). We remark that, as a first approximation, Ribberfors used for the solution of this equation the explicit expression given by his Eq. (40), which he called $p_{\min}$,

$$p_{\min} = \frac{\omega_1}{K}|1-\eta-\xi\eta|. \tag{57}$$

This expression follows from the exact equation (56) with $E(\tilde{\Delta}_{\min})$ replaced by 1. Although the difference between the exact $\tilde{\Delta}_{\min}$ in Eq. (55) and the approximate value $p_{\min}$ is not important at photon energies around the electron rest energy, the ER limits of $p_{\min}$ and of $\tilde{\Delta}_{\min}$ do differ as shown later. We will always work with the exact solution (55) of Eq. (56).

In contrast to the NRIA case, where the cross section is directly connected to the Compton profile, as shown in Eq. (A5), in RIA only an approximate result of that form is valid, given in Eq. (47) of [9] *for a spherical symmetric potential*

$$\sigma_2^{\mathrm{RIA}} \approx r_0^2 \frac{\eta}{2K} \frac{\bar{X}_{\mathrm{int}}(\omega_1,\xi,\eta;\tilde{\Delta}_{\min})}{E(\tilde{\Delta}_{\min})} J(\tilde{\Delta}_{\min}). \tag{58}$$

The Compton profile is

$$J(\tilde{\Delta}_{\min}) = 2\pi \int_{\tilde{\Delta}_{\min}}^{\infty} p\rho(p)dp \tag{59}$$

and the approximation (58) was obtained in Ribberfors [9] by an integration by parts in Eq. (53), dropping terms argued to be small. The validity of the approximation was confirmed by numerical calculations in the case of low Z atoms, but the assertions that the approximation is always good for backward scattering fail for high Z [18], where there are significant corrections to all angles. In writing Eq. (58), we use $\tilde{\Delta}_{\min}$, not $p_{\min}$ of Ribberfors, as we have discussed.

C. ER limit of RIA

Now we obtain the RIA expressions for TDCS and DDCS in the ER limit, as defined at the end of Sec. II. As mentioned in Sec. I, we shall use the superscript RIA-ER in referring to the ER limit of the RIA cross sections.

For TDCS, we need to consider Eq. (49). First of all, we have to determine the ER expression $\tilde{\Delta}_{\mathrm{ER}}$ for the magnitude of the momentum transfer $\tilde{\Delta}$, the variable of the cross section Σ_3 in Eq. (12). We start from the definition (41), giving for the magnitude $\tilde{\Delta}^2$,

$$\tilde{\Delta}^2 = (\tilde{p}-K)^2 + 4\tilde{p}K\sin^2\frac{\beta}{2}. \tag{60}$$

In order to see what happens to $\tilde{\Delta}$ in the ER limit, we need the behavior of the momentum $\tilde{p}$ and K in the ER limit. For K, the behavior is given by Eq. (19), where the second term is finite. The behavior of $\tilde{p}$ follows from Eq. (47) using the condition (20) according to which $\beta \to 0$ as $1/\omega_1$. As it follows that the dominant term for $\tilde{p}$ is the same as for K in Eq. (19), we have to include also, for both $\tilde{p}$ and K, the terms that are finite in the ER limit. A straightforward calculation leads to

$$\tilde{p} = (\omega_1-\omega_2) + \frac{1}{2}\left(s+\frac{1}{s}\right) + \frac{1}{2s}[(\Delta^{\mathrm{ER}})^2 - q^2] + O\left(\frac{1}{\omega_1}\right),$$

$$s \equiv \frac{\xi\eta}{1-\eta}, \quad q = s - E_0. \tag{61}$$

We have eliminated β from $\tilde{p}$ using the ER expression (21) of the physical momentum Δ^{ER} and, as a consequence, Δ^{ER} and q appear in the result. We notice that the dominant term, $\omega_1 - \omega_2$, is the same as that of the physical momentum in Eq. (16), whose value follows from the true energy conservation. Finally, we reach the connection between the ER limit of the fictitious value of the momentum transfer in Eq. (60), denoted by $\tilde{\Delta}^{\mathrm{ER}}$, and the ER limit of the true total momentum transfer magnitude Δ^{ER} in Eq. (21),

$$(\tilde{\Delta}^{\mathrm{ER}})^2 = \frac{1}{4s^2}\{[(\Delta^{\mathrm{ER}})^2 - q^2]^2 + 2[(\Delta^{\mathrm{ER}})^2 - q^2](1+s^2) + (s^2-1)^2\}, \tag{62}$$

a connection needed in order to compare results coming from RIA-ER to exact ER results.

Since, according to Eq. (22), $\Delta^{\mathrm{ER}} \geq |q|$ and as s in Eq. (61) is independent of Δ^{ER}, it follows that the minimum value of the fictitious total momentum transfer in the ER limit is reached for $\Delta^{\mathrm{ER}} = |q|$ and its expression is

$$(\tilde{\Delta}^{\mathrm{ER}}_{\min})^2 = \frac{(s^2-1)^2}{4s^2}$$

or, explicitly,

$$\tilde{\Delta}^{\mathrm{ER}}_{\min} = \left|\frac{s^2-1}{2s}\right| = \frac{|\xi^2\eta^2 - (1-\eta)^2|}{2\xi\eta(1-\eta)}. \tag{63}$$

The same result is obtained directly from expression (55), taking the ER limit, as it should be. We may also write the associated energy

$$E(\tilde{\Delta}^{\mathrm{ER}}_{\min}) = \sqrt{1+(\tilde{\Delta}^{\mathrm{ER}}_{\min})^2} = \frac{\xi^2\eta^2 + (1-\eta)^2}{2(1-\eta)\xi\eta} = \frac{s^2+1}{2s}. \tag{64}$$

A straightforward calculation, using Eq. (43), shows that the dominant term of the denominator in Eq. (49) behaves as $\omega_1\eta\xi$. This leads to the simple expression

$$\sigma_3^{\text{RIA-ER}} = \omega_1 \frac{r_0^2}{2} \frac{(1-\eta)^2}{\xi} X_0^{\text{ER}} \rho(\tilde{\Delta}^{\text{ER}}), \tag{65}$$

in which X_0^{ER}, obtained by taking the ER limit of $\tilde{R}_1$ and $\tilde{R}_2$ in Eq. (50),

$$\tilde{R}_1^{\text{ER}} = \omega_1 \frac{\xi\eta}{1-\eta}, \quad \tilde{R}_2^{\text{ER}} = \eta \tilde{R}_1^{\text{ER}}, \tag{66}$$

has the expression (36). Finally,

$$\sigma_3^{\text{RIA-ER}} = \omega_1 \frac{r_0^2}{2} (1-\eta)^2 \frac{1+\eta^2}{\xi\eta} \rho(\tilde{\Delta}^{\text{ER}}). \tag{67}$$

We shall be more interested in the cross section (12), for which

$$\Sigma_3^{\text{RIA-ER}} = \frac{1}{\omega_1} \frac{r_0^2}{2} \frac{1+\eta^2}{\xi\eta} \Delta^{\text{ER}} \rho(\tilde{\Delta}^{\text{ER}}). \tag{68}$$

We note that in this expression, the first factor is dependent only on the variables ξ and η, the second factor is Δ^{ER}, the true physical total momentum transfer, and that the third factor depends only on $\tilde{\Delta}^{\text{ER}}$, the argument of the momentum distribution, defined in Eq. (62) and depending on Δ^{ER}. The structure of TDCS will have implications for DDCS, as shown next.

One notices also the different behavior for extremely large ω_1 of the cross section $\sigma_3^{\text{RIA-ER}}$ in Eq. (67), which increases linearly with ω_1, and of $\Sigma_3^{\text{RIA-ER}}$, which decreases as $1/\omega_1$. This is connected with the decrease, with increasing ω_1, of the solid angle in which the electron momentum can be emitted [see Eq. (13)].

Now we consider *the ER limit of DDCS*. We can proceed in two ways: (i) take the ER limit of the result (53) or (ii) continue with the integration of the ER limit of TDCS. We describe the first approach and then mention how the second approach leads to the same result.

In Eq. (53), the dependence on ω_1 is contained in the photon transfer momentum K in front of the integral, in the integration limit $\tilde{\Delta}_{\text{min}}$, and in the function $\bar{X}_{\text{int}}$ under the integral. According to Eq. (19), the photon momentum transfer K goes to infinity as $\omega_1(1-\eta)$, as the second term is finite. The ER limit for $\tilde{\Delta}_{\text{min}}$ was already established in Eq. (63). Finally, if the expression for $\bar{X}_{\text{int}}$ is analyzed, as indicated in the Appendix, one finds that in the lowest order in $1/\omega_1$, the function becomes independent of $\tilde{\Delta}$,

$$\bar{X}_{\text{int}}(\omega_1, \xi, \eta; \tilde{\Delta}) = \frac{1+\eta^2}{\eta} + O\left(\frac{1}{\omega_1}\right) = X_0^{\text{ER}} + O\left(\frac{1}{\omega_1}\right), \tag{69}$$

and so it can be taken out of the integral. So the ER limit of $\bar{X}_{\text{int}}$ coincides with X_0^{ER} in Eq. (36) valid for scattering on a free electron.

From the previous equations, one then gets *the ER limit for the DDCS in RIA*, displaying the decrease of DDCS as $1/\omega_1$,

$$\sigma_2^{\text{RIA-ER}} = r_0^2 \frac{\pi}{\omega_1} \frac{1+\eta^2}{1-\eta} \int_{\tilde{\Delta}_{\text{min}}^{\text{ER}}}^{\infty} \frac{\tilde{\Delta}\rho(\tilde{\Delta})}{E(\tilde{\Delta})} d\tilde{\Delta}. \tag{70}$$

The integration limit vanishes for the free Compton frequency (29) when the ratio s defined in Eq. (62) becomes equal to 1. In conclusion, Eq. (70) is the ER limit of Eq. (53).

Before we comment on the result (70), we mention that the second approach to get the RIA-ER DDCS involves the integration of Σ_3 over the magnitude of the physical total momentum transfer

$$\sigma_2^{\text{RIA-ER}} = \int_{|q|}^{\infty} \Sigma_3^{\text{RIA-ER}} d\Delta^{\text{ER}}. \tag{71}$$

We use the result (68) and make a change of variable from Δ^{ER} to $\tilde{\Delta}^{\text{ER}}$. The two variables are connected by Eq. (62). Based on this and noting that the integration limit changes from $|q|$ for Δ^{ER} to $\tilde{\Delta}_{\text{min}}^{\text{ER}}$ for $\tilde{\Delta}^{\text{ER}}$, the expression (71) takes the form (70).

The main feature of DDCS multiplied by ω_1, in the RIA-ER approach, is the factorization as a product of a function of η only,

$$F(\eta) \equiv \frac{1+\eta^2}{1-\eta}, \tag{72}$$

with a function of $\tilde{\Delta}_{\text{min}}^{\text{ER}}$ only (and of the parameters which characterize the momentum distribution ρ). This is a general property of RIA that we will exploit in showing results in the particular case of scattering from the K shell of an electron in the Coulomb field. Given that the integrand is positive, the integral in Eq. (70) takes its largest value when the variable $\tilde{\Delta}_{\text{min}}^{\text{ER}}$, with the expression (63), vanishes. This happens for $s=1$, i.e., at the free Compton frequency (29), which is then the center point of the Compton peak in IA. We shall find below that the RIA-ER variable $\tilde{\Delta}_{\text{min}}^{\text{ER}}$ is also useful in characterizing the EC results.

Finally, we mention that in the high-energy limit Ribberfors' approximate relation (58) becomes

$$\sigma_2^{\text{RIA-ER}} \approx r_0^2 \frac{\pi}{\omega_1} F(\eta) \frac{1}{2\pi} \frac{J(\tilde{\Delta}_{\text{min}}^{\text{ER}})}{\sqrt{1+(\tilde{\Delta}_{\text{min}}^{\text{ER}})^2}} \equiv \sigma_2^{\text{CP-ER}}, \tag{73}$$

still showing the factorization, but now written in terms of the Compton profile, defined as in Eq. (A6) with the expression (59) for a central potential.

It is useful to note that the argument of the Compton profile $\tilde{\Delta}_{\text{min}}^{\text{ER}}$ with the expression (63) differs from what would be the ER limit of Ribberfors p_{min} in Eq. (57), equal to $|1-s|$. This means that the approximate expression p_{min} should not be used for very high photon energies. Nevertheless, for $s=1$, the two expressions vanish and for s near 1 (vicinity of the Compton line), the values of $\tilde{\Delta}_{\text{min}}^{\text{ER}}$ and p_{min} are close. For more details on this aspect, see [18].

D. Case of the 1*s* state of a hydrogenlike atom

Up to this point, the equations we have written are general equations, based on RIA, for a charge density with spherical

symmetry. In the following, we discuss the case of an electron bound in the K shell of a Coulomb potential with nuclear charge Z. Then, the total bound-electron energy is

$$E_0 \equiv \gamma = \sqrt{1-a^2}, \quad a \equiv \alpha Z. \tag{74}$$

In this case, the cross section (70) depends on a through the momentum distribution, which has a compact analytic expression; for $a^2 \ll 1$, it reduces to the NR expression in Eq. (A9). The integral in Eq. (70) can be performed analytically if the NR charge distribution is used. Assuming light and intermediate Z, we neglect terms of the order a^2, with the result

$$\omega_1 \sigma_2^{\text{RIA-ER}} = r_0^2 \frac{8a^5}{\pi} F(\eta) \left\{ \frac{E(\tilde{\Delta}_{\min}^{\text{ER}})}{6[(\tilde{\Delta}_{\min}^{\text{ER}})^2 + a^2]^3} + \frac{5}{32} \ln \frac{(\tilde{\Delta}_{\min}^{\text{ER}})^2 + a^2}{[E(\tilde{\Delta}_{\min}^{\text{ER}}) + 1]^2} \right\}, \quad a^2 \ll 1, \tag{75}$$

where $\tilde{\Delta}_{\min}^{\text{ER}}$ is given by Eq. (63).

Because, as shown in more detail in Sec. VII, the DDCS takes its largest values for $|\tilde{\Delta}_{\min}^{\text{ER}}| \leq a$, known as the Compton peak region, it is of interest to consider the behavior of DDCS for this case. The dominant term in Eq. (75) for $(\tilde{\Delta}_{\min}^{\text{ER}})^2 + a^2 \ll 1$ is the first term, from which one gets

$$\omega_1 \sigma_2^{\text{RIA-ER}} = \frac{4r_0^2}{3\pi} F(\eta) \frac{a^5}{[(\tilde{\Delta}_{\min}^{\text{ER}})^2 + a^2]^3}, \quad (\tilde{\Delta}_{\min}^{\text{ER}})^2 + a^2 \ll 1, \tag{76}$$

an expression which describes the dominant behavior of the hydrogenic ER limit of DDCS for low and medium values of the nuclear charge Z. We mention that the same result (76) is obtained using in the approximate result Eq. (73) the NR expression (A9) for CP and replacing the square root by 1.

V. EC-ER LIMIT FOR *K*-SHELL COMPTON SCATTERING

As mentioned in the Sec. I, for the case of the K shell of a hydrogenlike atom, it was possible [6] to derive an analytic expression for the ER limit of the Compton scattering amplitude and from it to obtain TDCS and DDCS. Reference [6] contains a detailed description of the calculation and also graphs of DDCS resulting from the numerical evaluation of the analytic expressions. Some corresponding predictions for TDCS are given in [7]. There is also [16], concerned with the soft-photon limit at high energies, which is handled separately because it cannot be included in the general equations of the ER limit, as we have described them.

The basic result of EC-ER is the analytic expression Eq. (91) of [6] for the multiply differential cross section Σ_3, defined in Eq. (12) here, which gives the distribution in the scattered photon observables (frequency and direction) and in the magnitude of the total momentum transfer. In our paper, we have already introduced a distinct notation Δ^{ER} for Δ in the ER limit; the meaning of Δ in [6] and of Δ^{ER} here is the same. According to Eq. (22), this is a variable restricted by $\Delta^{\text{ER}} \geq |q|$ and its connection with the electron-scattering angle β follows from Eqs. (21) and (20). In agreement with the more general expression in Eq. (21), for the Coulomb K shell, the variable q is now

$$q = \frac{\xi\eta}{1-\eta} - \gamma = s - \gamma, \tag{77}$$

with γ given by Eq. (74) and s defined in Eq. (61).

The cross section $\Sigma_3^{\text{EC-ER}}$ decreases as $1/\omega_1$ and does not depend on the azimuthal angle Φ of the total momentum transfer in a reference frame with the third axis along the photon momentum transfer. This leads to the ER result for DDCS,

$$\sigma_2^{\text{EC-ER}} \equiv \frac{d^2\sigma_{\text{EC-ER}}}{d\omega_2 d\Omega_2} = 2\pi \int_{|q|}^{\infty} \Sigma_3^{\text{EC-ER}} d\Delta^{\text{ER}}. \tag{78}$$

We emphasize that, according to the ER equations, due to the behavior of the cross section Σ_3^{ER}, the initial photon energy ω_1 appears only as the factor $1/\omega_1$ in DDCS; this is the same behavior found in RIA in the previous section.

As derived in [6], the analytic expression for $\Sigma_3^{\text{EC-ER}}$ is not simple: it involves three Appell functions F_1, with the dependence on a appearing both in the parameters of the functions and also in the two of the three variables of these functions. The integration over Δ^{ER} for DDCS has to be done numerically. We express the factor $1/\xi$ in Eq. (91) of [6] in terms of q and η, using Eq. (77), and we rewrite this equation in the form

$$\Sigma_3^{\text{EC-ER}} = \frac{r_0^2}{\omega_1} \frac{1+\eta^2}{1-\eta} \frac{\Delta^{\text{ER}}}{q+\gamma} T. \tag{79}$$

The function T depends only on a, q, and Δ^{ER}. As a result, we now identify one of the main features of the EC-ER limit, not discussed or exploited in [6]. If one takes as variables η and q, instead of η and ξ, then the structure of the analytic results reveals the factor $(1+\eta^2)/(1-\eta)$ [the same factor Eq. (72) as in RIA-ER] that multiply a function of a, q, and Δ^{ER} for TDCS and a function of a and q only for DDCS, corresponding to what we have found in RIA-ER.

The correspondence between the variables in EC-ER and RIA-ER and the consequences of the structure described above are discussed in Sec. VI. In particular, one is led to a more compact representation of the EC-ER results, as illustrated in Sec. VII. We conclude this section by mentioning some simple expressions derived from EC-ER analytic results for small values of a.

For $a^2 \ll 1$, the analytic expression of T in Eq. (79) drastically simplifies and the following expression of Σ_3 follows:

$$\omega_1 \Sigma_3^{\text{EC-ER}} = r_0^2 \frac{a^5}{\pi^2} F(\eta) S(a) e^{2a\psi} \frac{\Delta^{\text{ER}}}{1+q} \left\{ \frac{4(1+q)}{[(\Delta^{\text{ER}})^2 + a^2]^4} + \frac{4q+3q^2}{(q^2+a^2)[(\Delta^{\text{ER}})^2 + a^2]^3} + \frac{1}{(q^2+a^2)[(\Delta^{\text{ER}})^2 + a^2]^2} \right\}, \quad a^2 \ll 1, \tag{80}$$

with $S(a)$ following from Eqs. (101) and (108) and ψ from Eq. (106) of [6], as

$$S(a) = \frac{2^{2\gamma}}{(1+\gamma)\Gamma(1+2\gamma)} \frac{2\pi a}{1-e^{-2\pi a}} \times \left| \frac{\Gamma(2+\gamma-ia)}{\Gamma(3-ia)} \right|^2 \left(\frac{a^2}{q^2+a^2} \right)^{\gamma-1}, \tag{81}$$

$$\tan\psi = -a/q, \quad -\pi \le \psi \le 0. \tag{82}$$

In fact, $S(a)$ depends also on q. Strictly, for $a=0$, both S and $e^{2a\psi}$ become equal to 1, but as the last exponential, as well as the factor $e^{-2\pi a}$ in $S(a)$ have quite large exponents, they depart quickly from 1, so they are kept in Eq. (80).

The result given in Eq. (80) was not written explicitly in [6]. The integration over Δ^{ER} of this expression leads to Eq. (109) of [6] that we reproduce here

$$\omega_1 \sigma_2^{\mathrm{EC\text{-}ER}} = r_0^2 \frac{a^5}{6\pi} F(\eta) \frac{S(a) e^{2a\psi}}{(q^2+a^2)^3} \frac{8+20q+15q^2}{1+q}, \quad a^2 \ll 1. \tag{83}$$

A simple calculation shows that, with the neglect of terms of the order a^4, the maximum of the approximate cross section (83) is located at $q=7a^2/12$.

If $(\Delta^{\mathrm{ER}})^2+a^2 \ll 1$ then $|q| \ll 1$ and the EC-ER result (80) reduces to

$$\omega_1 \Sigma_3^{\mathrm{EC\text{-}ER}} \approx r_0^2 \frac{4a^5}{\pi^2} F(\eta) S(a) e^{2a\psi} \frac{\Delta^{\mathrm{ER}}}{[(\Delta^{\mathrm{ER}})^2+a^2]^4}. \tag{84}$$

Taking into account all the approximations made, the last formula is valid for $|q| \ll 1$ and $(\Delta^{\mathrm{ER}})^2+a^2 \ll 1$.

Integration on Δ^{ER} and multiplication with 2π (for the integration on Φ) gives

$$\omega_1 \sigma_2^{\mathrm{EC\text{-}ER}} \approx r_0^2 \frac{4a^5}{3\pi} F(\eta) S(a) e^{2a\psi} \frac{1}{(q^2+a^2)^3}. \tag{85}$$

This result follows also directly from Eq. (83), neglecting q and q^2.

VI. COMPARISON OF THE ANALYTIC RESULTS OF RIA-ER AND EC-ER

Now we want to compare in more detail RIA-ER and EC-ER results for DDCS and also for TDCS. At the level of analytic equations, comparison can be made only in the small a case, as the EC analytic results [6], valid for any Z, are known only in terms of Appell functions for TDCS.

We refer first to DDCS. In the ER regime, in both RIA and EC cases, we have already noticed the factorization of the function $F(\eta)$ defined in Eq. (72) in the expression of DDCS. In the EC-ER case, as noticed in Sec. V, the variables in the factor multiplying F are q, defined in Eq. (77), and a. In the RIA-ER case, the only variables in the corresponding factor are $\tilde{\Delta}_{\mathrm{min}}^{\mathrm{ER}}$, defined in Eq. (63), and γ, defined in Eq. (74) and hidden in the momentum charge distribution. The variables of the two approaches, q and $\tilde{\Delta}_{\mathrm{min}}^{\mathrm{ER}}$, are connected, as shown in the following, a property that will be exploited in this section and in the presentation of numerical data. Using the expressions of Eqs. (63) and (77), one finds that $\tilde{\Delta}_{\mathrm{min}}^{\mathrm{ER}}$ follows from q as

$$\tilde{\Delta}_{\mathrm{min}}^{\mathrm{ER}} = \frac{|(q+\gamma)^2-1|}{2(q+\gamma)}. \tag{86}$$

For $a^2 \ll 1$ and $|q| \ll 1$, we get $\tilde{\Delta}_{\mathrm{min}}^{\mathrm{ER}} \approx |q|$.

Solving the second-order equation in Eq. (86) for $q+\gamma$, one finds the explicit expression of the two values of q that correspond to a given value of $\tilde{\Delta}_{\mathrm{min}}^{\mathrm{ER}}$,

$$q_{\mp} = -\gamma \mp \tilde{\Delta}_{\mathrm{min}}^{\mathrm{ER}} + \sqrt{1+(\tilde{\Delta}_{\mathrm{min}}^{\mathrm{ER}})^2}, \quad 0 \le \tilde{\Delta}_{\mathrm{min}}^{\mathrm{ER}} < \infty. \tag{87}$$

The first sign corresponds to the region $-\gamma \le q \le 1-\gamma$; the second sign to $q \ge 1-\gamma$. Note that to $q=0$ corresponds to the positive value $\tilde{\Delta}_{\mathrm{min}}=a^2/(2\gamma)$.

From Eq. (86), we also get the exact relation,

$$(\tilde{\Delta}_{\mathrm{min}}^{\mathrm{ER}})^2 + a^2 = (q^2+a^2) \frac{(2\gamma+q)^2+a^2}{4(\gamma+q)^2}, \tag{88}$$

that will be used in the comparison of analytic results valid in the small a case.

The comparison of the results coming from the two approaches can be done if we use the same variable. Our option for the variable used in comparing RIA-ER and EC-ER is $\tilde{\Delta}_{\mathrm{min}}^{\mathrm{ER}}$. Even more convenient is to let this variable to take also negative values. In this case, the limit of integration for RIA-ER DDCS in Eq. (70) is $|\tilde{\Delta}_{\mathrm{min}}^{\mathrm{ER}}|$, transforming $\sigma_2^{\mathrm{RIA\text{-}ER}}$ in an even function of the new variable. The extension of the range of $\tilde{\Delta}_{\mathrm{min}}^{\mathrm{ER}}$ allows the two relations (87) to be written in a single one

$$q = -\gamma + \tilde{\Delta}_{\mathrm{min}}^{\mathrm{ER}} + \sqrt{1+(\tilde{\Delta}_{\mathrm{min}}^{\mathrm{ER}})^2}, \quad -\infty < \tilde{\Delta}_{\mathrm{min}}^{\mathrm{ER}} < \infty. \tag{89}$$

The negative values of $\tilde{\Delta}_{\mathrm{min}}^{\mathrm{ER}}$ cover the region $-\gamma \le q \le 1-\gamma$.

In a representation of DDCS as a function of $\tilde{\Delta}_{\mathrm{min}}^{\mathrm{ER}}$, the EC-ER cross section is not symmetric with respect to $\tilde{\Delta}_{\mathrm{min}}^{\mathrm{ER}}=0$, unlike the extended RIA-ER cross section; the two values (q_-, q_+) of the variable q associated to a pair of values $(-|\tilde{\Delta}_{\mathrm{min}}^{\mathrm{ER}}|, |\tilde{\Delta}_{\mathrm{min}}^{\mathrm{ER}}|)$ are different and so are the corresponding values of the EC-ER cross sections. One has $q_+ - q_- = 2|\tilde{\Delta}_{\mathrm{min}}^{\mathrm{ER}}|$. The asymmetry of EC-ER results increases with Z.

Figures 1–3 in next section illustrate the previous discussion. Here we focus on the analytic expressions. As mentioned before, a comparison at the level of analytic results can be done only in the small a case. More precisely, we can compare the approximate results (76) and (85). It follows an expression for the ratio of the approximate cross sections in RIA-ER and EC-ER

$$\frac{\sigma_2^{\mathrm{RIA\text{-}ER}}}{\sigma_2^{\mathrm{EC\text{-}ER}}} \approx \frac{e^{-2a\psi}}{S(a)} \left(\frac{q^2+a^2}{(\tilde{\Delta}_{\mathrm{min}}^{\mathrm{ER}})^2+a^2} \right)^3. \tag{90}$$

Using the relation (88), we get

$$\frac{\sigma_2^{\text{RIA-ER}}}{\sigma_2^{\text{EC-ER}}} \approx \left(\frac{\gamma}{\gamma+q} + \frac{a^2+q^2}{4(\gamma+q)^2}\right)^3 \to 1, \quad a^2 \ll 1, \quad |q| \ll 1. \tag{91}$$

The factors $S(a)$ and $e^{-2a\psi}$ were replaced by 1 in the last step. Given the approximations made in order to get the same analytic expressions from the two approaches, it is to be expected that their predictions will not differ much in the peak region for small and intermediate values of the nuclear charge Z.

Now we refer to the comparison of analytic results for TDCS. If we compare first the structures of the EC-ER and RIA-ER results, we now show that the factor $F(\eta)$ defined in Eq. (72) is present in both cases. For the EC-ER case, this factor is already visible in the expression Eq. (79) of the cross section $\Sigma_3^{\text{EC-ER}}$, where the remaining factor depends on a,q and the variable of the angular distribution, Δ^{ER} in Eq. (21). The RIA-ER result for TDCS is given by Eq. (68) and, in order to see $F(\eta)$, it needs to be transcribed using Eq. (77), with the result

$$\omega_1 \Sigma_3^{\text{RIA-ER}} = \frac{r_0^2}{2} F(\eta) \frac{\Delta^{\text{ER}}}{\gamma+q} \rho(\tilde{\Delta}^{\text{ER}}). \tag{92}$$

The variables Δ^{ER} (the physical momentum transfer in the ER regime) and $\tilde{\Delta}^{\text{ER}}$, which appear in the charge distribution, are connected by Eq. (62), where in the present case, s and q are related as in Eq. (77).

For $a^2 \ll 1$, the previous expression (92) can be compared to the EC-ER expression (84). We get

$$\frac{\Sigma_3^{\text{RIA-ER}}}{\Sigma_3^{\text{EC-ER}}} \approx \frac{\pi^2}{8a^5} \frac{[(\Delta^{\text{ER}})^2 + a^2]^4}{\rho(\tilde{\Delta}^{\text{ER}})}, \quad (\Delta^{\text{ER}})^2 + a^2 \ll 1. \tag{93}$$

The factors $S(a)$ and $e^{2a\psi}$ have been replaced by 1, which we have noted as a poor approximation even for small a.

If the relativistic momentum distribution is replaced by its nonrelativistic limit (A9), we get

$$\frac{\Sigma_3^{\text{RIA-ER}}}{\Sigma_3^{\text{EC-ER}}} \approx \left(\frac{(\Delta^{\text{ER}})^2 + a^2}{(\tilde{\Delta}^{\text{ER}})^2 + a^2}\right)^4, \quad (\Delta^{\text{ER}})^2 + a^2 \ll 1. \tag{94}$$

In general, the variable $\tilde{\Delta}^{\text{ER}}$ is not identical with the variable Δ^{ER}, as shows the connection (62) of the two variables. Only for small values of Δ^{ER}, which imply also small values of $|q|$ already used in the EC-ER expression, these variables coincide. But, as these conditions are satisfied in the region near the Compton maximum for the corresponding angular distributions, the ratio (94) will be near 1.

From this section, we keep two conclusions: (i) it is useful to work with the same variables in presenting and comparing the EC and RIA results in the ER limit; (ii) we expect good agreement near the Compton peak, for not too high values of Z, for both DDCS and TDCS.

VII. NUMERICAL RESULTS AND DISCUSSION

The numerical results which we present refer to the Coulomb $1s$ electron. The analytic results displayed in the previous sections show that it is useful to study the scaled cross sections

$$\Sigma_3^{\text{sc}} \equiv \frac{\Sigma_3}{F(\eta)\sigma_0}, \quad \sigma_2^{\text{sc}} \equiv \frac{\sigma_2}{F(\eta)\sigma_0}, \tag{95}$$

where

$$\sigma_0 = \frac{4r_0^2}{3\pi a \omega_1}. \tag{96}$$

They are dimensionless due to the scaling factor σ_0 already used in [6]. From these functions, one can obtain the triply and doubly differential cross sections in their dependence on the variables with physical significance.

We first focus on DDCS. At fixed Z, the scaled function σ_2^{sc}, as given by the analytic formulas established in [6], depends only one variable q in Eq. (77). But, from Sec. IV, we know that we can use as variable $\tilde{\Delta}_{\text{min}}^{\text{ER}}$ defined in Eq. (63). All the EC-ER data shown in the figures are based on the analytic expression given in Eq. (91) of [6].

We begin by presenting now the EC-ER results in Fig. 1. In order to see the difference between the two possible choices for the variable, we use q/a in Fig. 1(a) and $\tilde{\Delta}_{\text{min}}^{\text{ER}}/a$ in Fig. 1(b). Both variables are dimensionless. We remind that the variables q and $\tilde{\Delta}_{\text{min}}^{\text{ER}}$ are given by Eqs. (77) and (63), respectively. The use of the factor $1/a$ in the two variables leads to a better presentation of the features of the results. Six values of Z ranging from 13 to 137 are considered in Fig. 1.

The vicinity of the limit $q=-\gamma$ corresponds to values of η near 0, not covered by the ER approximation. In this limit, the cross section increases. However, this increase, while showing the proper infrared rise tendency, is not quantitatively correct. In order to get the correct result in the infrared region, one must proceed as in [16]. The increase is visible in Fig. 1(a) only in the cases of large Z (82, 100, and 137). For $Z=137$, the limit for q/a is near 0, for $Z=100$ it is -0.94, and for $Z=82$, this limit -1.34. All the other graphs would also show this increase near their corresponding minimum value for q, which means large negative q/a for small Z.

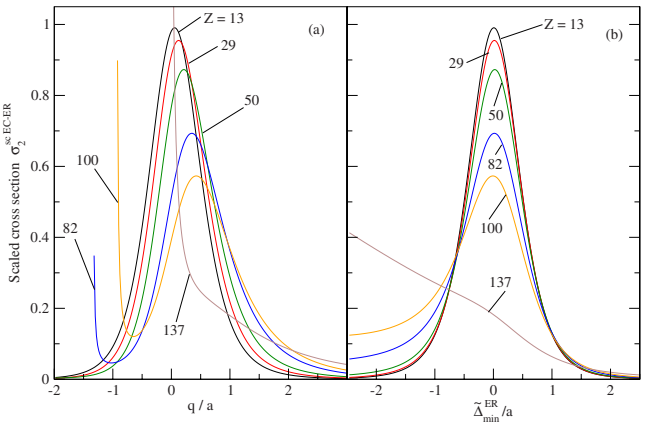

FIG. 1. (Color online) Scaled EC-ER DDCS for several values of Z, as function of the variable q/a in (a) and of $\tilde{\Delta}_{\text{min}}^{\text{ER}}/a$ in (b). The variables are dimensionless [see Eqs. (63), (74), and (77)].

We also mention that, according to Eq. (77), the value $q=-\gamma$ is also reached for $\xi=0$, a special point not included in the ER-EC results because there a change of the order of magnitude of the amplitude from $O(1/\sqrt{\omega_1})$ to $O(1)$ arises, as discussed after Eq. (84) in [6].

In Fig. 1(b), the same results are presented using the variable $\tilde{\Delta}^{\mathrm{ER}}_{\mathrm{min}}/a$. The finite region $(-\gamma, 1-\gamma)$ on the q scale is shifted in the infinite region $(-\infty, 0)$ on $\tilde{\Delta}^{\mathrm{ER}}_{\mathrm{min}}/a$ scale and a slight asymmetry about $\tilde{\Delta}^{\mathrm{ER}}_{\mathrm{min}}=0$ becomes visible as Z is increased, in contrast to RIA-ER case, shown in Fig. 2. Now, due to the choice of the variable, not only the curves for low Z are almost symmetric, but also the region of increase is not seen, being shifted far to the left.

We remark that Figs. 1(a) and 1(b) represent different and more compact ways than that used in [6] for presenting the EC-ER results. In the quoted paper, data were displayed using the variables ξ and η in Eq. (8), either as function of ξ at fixed η or as function of η at fixed ξ. Now, we can say that all the information contained in the graphs of [6] are concentrated in either Fig. 1(a) or 1(b), as from a curve which gives, for given Z, the dependence of DDCS as a function of q/a or, alternatively, of $\tilde{\Delta}^{\mathrm{ER}}_{\mathrm{min}}/a$, the photon spectral distributions, i.e., σ_2 as function of η at fixed values of ξ, and the photon angular distributions, i.e., σ_2 as function of ξ at fixed values of η, can be both obtained using the expression (77) or (63). Of course, the factor $F(\eta)$ must be included.

The maximum of the graphs in Fig. 1(b) is located near $\tilde{\Delta}^{\mathrm{ER}}_{\mathrm{min}}=0$. This position corresponds to a value $1-\gamma$ for q which implies $\xi\eta=1-\eta$. This is exactly the condition (29) which corresponds to the Compton line in the free-electron case. But, in fact, as already mentioned in Sec. V, for low Z the maximum is located at $q=7a^2/12$. In the variable used in Fig. 1(b), this corresponds to $\tilde{\Delta}^{\mathrm{ER}}_{\mathrm{min}}=a^2/12$. This is *the shift* of the EC-ER DDCS maximum for small a^2 compared to the free-electron and RIA-ER cases.

In Fig. 2, which presents RIA-ER results, the dashed curve represents the scaled cross section associated with the approximation (76), which is simply $[1+(\tilde{\Delta}^{\mathrm{ER}}_{\mathrm{min}}/a)^2]^{-3}$, a function independent of Z when the variable $\tilde{\Delta}^{\mathrm{ER}}_{\mathrm{min}}/a$ is used. The curve for $Z=13$ is not shown because on our figure, it would be hard to distinguish it from the dashed curve.

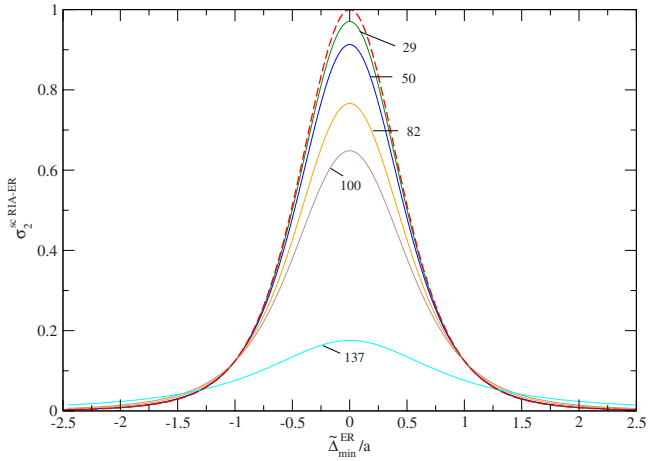

FIG. 2. (Color online) Scaled RIA-ER DDCS for several values of Z as function of the dimensionless variable $\tilde{\Delta}^{\mathrm{ER}}_{\mathrm{min}}/a$ [see Eqs. (63) and (74)].

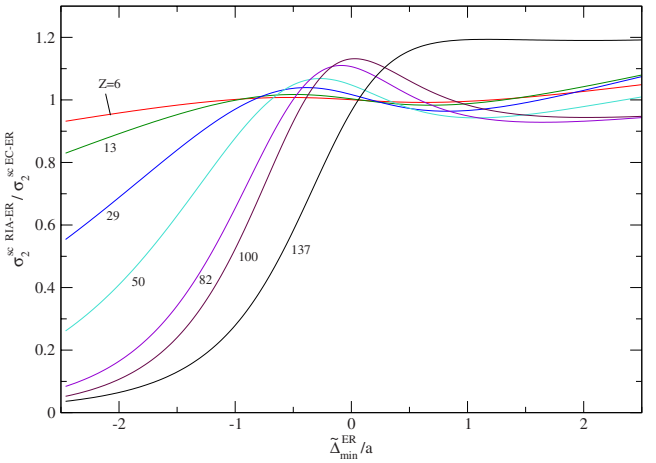

FIG. 3. (Color online) Ratio of RIA-ER and EC-ER as a function of $\tilde{\Delta}^{\mathrm{ER}}_{\mathrm{min}}/a$.

In order to compare quantitatively EC-ER and RIA-ER results, we show in Fig. 3 the ratio $\sigma_2^{\mathrm{RIA\text{-}ER}}/\sigma_2^{\mathrm{EC\text{-}ER}}$, as a function of $\tilde{\Delta}^{\mathrm{ER}}_{\mathrm{min}}/a$, for various Z. In the region $(-0.5, 0.5)$ of the variable, we have found relative differences less than 2% for $Z=13$, less than 4% for $Z=29$, up to 6% for $Z=50$, and up to 12% for $Z=82$. Outside this region, the relative error increases for negative values of the variable, but not for positive values. Based on all these, we conclude that RIA-ER is a good approximation of the EC-ER results for low Z values and it is handling fairly well high Z effects in the Compton peak region.

In Fig. 4, we test in the ER regime the validity within the relativistic impulse approximation of the approximate relation that connects DDCS with CP. We plot the ratio of the quantities $\sigma_2^{\mathrm{CP\text{-}ER}}$ in Eq. (73) and $\sigma_2^{\mathrm{RIA\text{-}ER}}$. We see that the approximation works quite well for $|\tilde{\Delta}^{\mathrm{ER}}_{\mathrm{min}}|/a \leq 1$.

We have also calculated TDCS, for which [6] did not give numerical results. Only in [7] one can find several graphs for

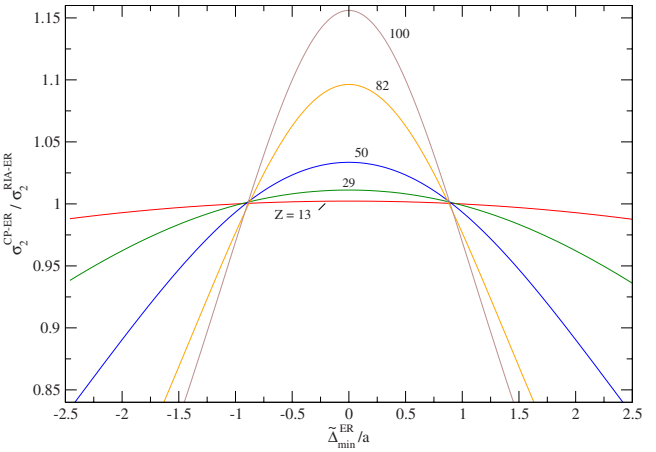

FIG. 4. (Color online) Ratio of DDCS evaluated in terms of the Compton profile [Eq. (73)] and with RIA-ER [Eq. (70)] in their dependence on $\tilde{\Delta}^{\mathrm{ER}}_{\mathrm{min}}/a$.

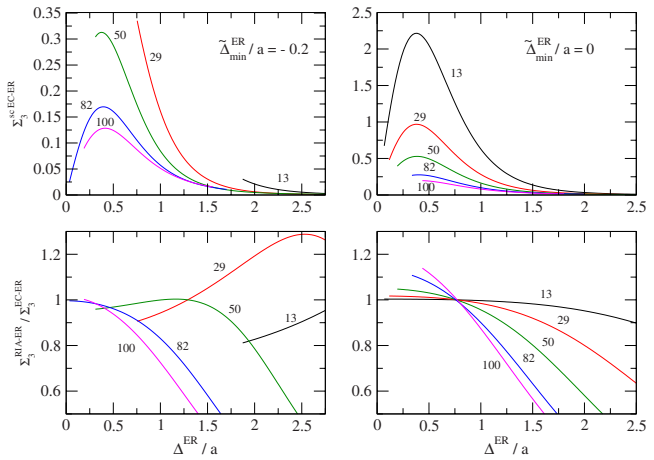

FIG. 5. (Color online) EC-ER TDCS (upper panels) and ratio of TDCS in RIA-ER and EC-ER approaches (lower panels) as a function of Δ^{ER}/a with Δ^{ER} the total momentum transfer magnitude. Results for different values of Z are shown at $\tilde{\Delta}^{ER}_{min}/a=-0.2$ and 0.

the quantity Σ_3 in Eq. (12), as a function of Δ (identical with Δ^{ER} here), for $Z=13$, 29, 50, and 82, in the vicinity of the Compton peak. Our Figs. 5 and 6 illustrate the behavior of EC-ER results and the comparison of EC-ER and RIA-ER predictions for TDCS. In the upper panels, the scaled EC-ER TDCS is shown as function of Δ^{ER}/a for fixed values of $\tilde{\Delta}^{ER}_{min}/a$, taken near the maximum of DDCS, and for five values of Z. In the lower panels, the ratio of the cross sections $\sigma_3^{RIA\text{-}ER}/\sigma_3^{EC\text{-}ER}$ is represented. In Fig. 5, the left panels and right panels correspond, respectively, to the values −0.05 and 0 for and $\tilde{\Delta}^{ER}_{min}/a$. In Fig. 6, the values for the last quantity are 0.05 in the panels on the left and 0.1 in the panels on the right. The starting point of each curve is fixed by the restriction (22). We see that in all cases we have shown, the values of TDCS coming from the two approaches have the same behavior as the DDCS, namely, they agree better as Z becomes smaller.

More work is needed in order to analyze the TDCS in RIA, in both ER limit and at finite photon energies, as the first studies at finite energies show that in many cases, IA

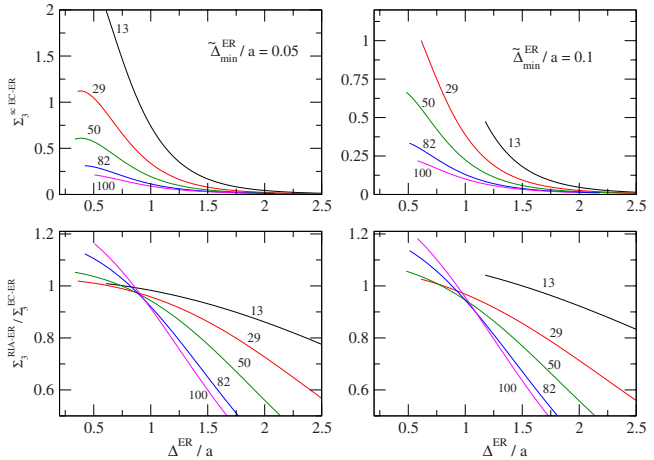

FIG. 6. (Color online) Same as Fig. 5, but for $\tilde{\Delta}^{ER}_{min}/a=0.05$ and 0.1.

describes well the DDCS but not the TDCS [4,10,19]. The results of the present work, in which the ER of RIA for the $1s$-Coulomb electron was compared to ER-EC results, together with the studies at photon energies in the range comparable to or larger than the electron rest energy [5], give support to the view that RIA is a reasonable approximation at high photon energies, at least for small and medium values for Z. In order to see how soon the actual ER limit results become adequate, we have computed RIA results with Eq. (53), valid at any photon energy, and we have compared them to RIA-ER results obtained from Eq. (70). In this comparison, not shown here, we have found that the photon energy has to be very high (at least 50 times the electron rest mass energy) in order to approach the ER limit, i.e., the asymptotic $1/\omega_1$ behavior is reached slowly. Given this situation, we suggest a possible procedure to use RIA and EC-ER results to predict DDCS at finite energies (where EC-ER results are not valid) and high Z (where RIA starts to become incorrect), having in mind that the terms neglected by EC-ER are of the order $1/\omega_1$, and are important, and those neglected by RIA are of the order $(\alpha Z)^2$. Given the parameters Z and ω_1, and the values of θ and ω_2 for which one wants to predict DDCS, one calculates first σ_2^{RIA} using the Ribberfors formula (53). Then one determines the corresponding variables ξ and η, according to Eq. (8), and using them, one calculates the ER cross sections, $\sigma_2^{RIA\text{-}ER}$ and $\sigma_2^{EC\text{-}ER}$. Then, with an error of order $(\alpha Z)^2/\omega_1$, the proposed value for the cross section will be

$$\sigma_2 = \sigma_2^{RIA}\frac{\sigma_2^{EC\text{-}ER}}{\sigma_2^{RIA\text{-}ER}}. \tag{97}$$

We note that given ξ and η, as the corresponding ω_2 and θ,

$$\kappa_2 = \eta\omega_1, \quad \cos\theta = 1 - \xi/\omega_1, \tag{98}$$

depend also on ω_1, the same $\sigma_2^{EC\text{-}ER}$ and $\sigma_2^{RIA\text{-}ER}$ are needed for various pairs of ω_2 and θ and different ω_1. This is not true for σ_2^{RIA} in Eq. (97). The larger the ω_1 will be, the better will be the prediction.

VIII. CONCLUSIONS

In summary, in this paper devoted to very high-energy Compton scattering on a bound electron, we have investigated the ER limit of RIA and compared to exact Coulomb results valid in the ER limit. The paper contains two contributions to RIA general equations for Compton scattering from a s state: (i) the analytic expression of the TDCS in RIA, for any photon energy, Eq. (49), and (ii) a high-energy limit of TDCS and DDCS, Eqs. (67) and (70), respectively, obtained applying the same rules as in the ER calculation of [6] for the Coulomb K-shell case.

We have noticed the similar structures of RIA-ER and EC-ER analytic expressions of TDCS, in which, apart from the $1/\omega_1$ factor, the dependence on photon frequencies is contained in the simple function (72) depending on the photon frequency ratio ω_2/ω_1 only. The function left after factorization depends on αZ, on an angular variable Δ_{ER} and on

another variable, which is different in the two cases, $\tilde{\Delta}_{\min}^{\mathrm{ER}}$ in Eq. (55) for RIA-ER and q in Eq. (77) for EC-ER. This structure is transferred to DDCS, where the variable Δ^{ER} disappears by integration. The specific variables, q of EC-ER and $\tilde{\Delta}_{\min}^{\mathrm{ER}}$ of RIA-ER, are connected by Eq. (86).

We have exploited these remarks, using the variable $\tilde{\Delta}_{\min}^{\mathrm{ER}}$, the variable proper to ER of RIA, in displaying the results for DDCS. In particular, Fig. 1(b) is a more compact way of presentation than in [6]. The use of the same variable allows to see in a better way how the EC-ER and RIA-ER results coincide in the peak region in the limit $Z\rightarrow 0$ and how the departure from RIA manifests in the asymmetry of the graphs about the maximum and in the maximum shift which become larger with increasing Z.

We have established by comparison to EC-ER numerical results the error introduced by RIA in the ER limit; the relative difference increases with Z, but, in the peak region it stays below 15% for $Z\simeq 100$. So RIA-ER handles the high Z case fairly well.

We have suggested how to use RIA and EC-ER results to make predictions at finite energies and not necessarily low Z. An extended analysis of TDCS is needed in order to understand more deeply their properties.

The conclusion of our work is that RIA is a reliable approximation in describing the peak region in the high-energy regime of Compton scattering by K-shell bound electrons, but small deviations, growing with Z, persist in the high-energy limit.

ACKNOWLEDGMENTS

This work has been supported in part by Grant No. NSF-0456499 and the Romanian Grant No. CEEX-D11-56-05. One of the authors (V.F.) thanks Madalina Boca for her assistance in the preparation of the paper.

APPENDIX: DETAILS ON IA

In the first part of this appendix, we review the basic equations of NRIA, which are to be compared to the corresponding relativistic equations of our text. In the second part, we give some details of the RIA case. All the cross sections are averaged/summed over the initial/final particle (electron and photon) polarizations.

1. NRIA results

In the *nonrelativistic case*, the most differential cross section for the scattering on a free electron, averaged on initial and summed-over final polarizations of the electron and photon, is

$$d^4\sigma_{\mathrm{NR}} = \frac{1+\cos^2\theta}{2}\frac{\omega_2}{\omega_1}\delta(\mathbf{p}-\mathbf{p}_0-\mathbf{K}) \times \delta\left(\frac{p^2}{2}-\frac{p_0^2}{2}-\omega_1+\omega_2\right)d\omega_2 d\Omega_2 d\mathbf{p}, \quad \text{(A1)}$$

from which the impulse-approximation result follows by integrating over a distribution of initial momenta $\mathbf{p}_0$,

$$d^4\sigma_{\mathrm{NR\text{-}IA}} = \frac{1+\cos^2\theta}{2}\frac{\omega_2}{\omega_1}|\rho_{\mathrm{NR}}(\mathbf{p}-\mathbf{K})|^2 \times \delta\left(\frac{p^2}{2}-\frac{(\mathbf{p}-\mathbf{K})^2}{2}-\omega_1+\omega_2\right)d\omega_2 d\Omega_2 d\mathbf{p}, \quad \text{(A2)}$$

with $\rho_{\mathrm{NR}}(\mathbf{p})=|\phi(\mathbf{p})|^2$ and ϕ the Fourier transform of the initial wave function of the bound electron. The fictitious momentum magnitude attributed by the δ function to the final electron is

$$\tilde{p}_{\mathrm{NR}} = \frac{K^2/2+\omega_1-\omega_2}{K\cos\beta}, \quad \text{(A3)}$$

where β is the angle between $\mathbf{p}$ and $\mathbf{K}$. This relation is the nonrelativistic analog of Eq. (43) and (47).

Integrating over the magnitude of the momentum in Eq. (A2) leads to the nonrelativistic triply differential cross section

$$\sigma_3^{\mathrm{NR\text{-}IA}} = \frac{1+\cos^2\theta}{2}\frac{\omega_2}{\omega_1}\frac{\tilde{p}_{\mathrm{NR}}^2}{K\cos\beta}|\rho_{\mathrm{NR}}(\tilde{\mathbf{p}}-\mathbf{K})|^2, \quad \beta<\pi/2, \quad \text{(A4)}$$

where the vector $\tilde{\mathbf{p}}$ has the magnitude $\tilde{p}_{\mathrm{NR}}$.

The DDCS follows by integrating over the electron-momentum direction. This leads to

$$\sigma_2^{\mathrm{NR\text{-}IA}} = \frac{1+\cos^2\theta}{2}\frac{\omega_2}{\omega_1}\frac{1}{K}J_{\mathrm{NR}}(p_z), \quad \text{(A5)}$$

where J is the Compton profile, with the general definition

$$J_{\mathrm{NR}}(p_z) \equiv 2\pi\int_{-\infty}^{\infty}\int_{-\infty}^{\infty}\rho_{\mathrm{NR}}(p_x,p_y,p_z)dp_x dp_y \quad \text{(A6)}$$

and

$$p_z = \frac{K}{2}-\frac{\omega_1-\omega_2}{K}. \quad \text{(A7)}$$

For a charge density with spherical symmetry, one is left with the single integral

$$J_{\mathrm{NR}}(p_z) \equiv \int_{p_z}^{\infty} p\rho_{\mathrm{NR}}(p)dp. \quad \text{(A8)}$$

In the case of the K shell of a hydrogenlike atom, the NR charge density and the Compton profile are

$$\rho_{\mathrm{NR}}^{\mathrm{K}}(p) = \frac{8a^5}{\pi^2(p^2+a^2)^4}, \quad J_{\mathrm{NR}}^{\mathrm{K}}(p_z) = \frac{8a^5}{3\pi(p_z^2+a^2)^3}. \quad \text{(A9)}$$

2. RIA results

The quantity $\bar{X}_{\mathrm{int}}$ in Eq. (53) is given by Eq. (37) of [9], which we give here for the sake of completeness, with slightly different notations

$$\bar{X}_{\text{int}}(\omega_1;\xi,\eta;\tilde{\Delta}) = 2 + C\left(\frac{1}{(A_0^2 - B^2)^{1/2}} - \frac{1}{(A^2 - B^2)^{1/2}}\right) + \frac{C}{\omega_1^2}\left(\frac{A_0}{(A_0^2 - B^2)^{3/2}} + \frac{A}{(A^2 - B^2)^{3/2}}\right), \tag{A10}$$

where

$$C = W - \frac{2}{\omega_1} - \frac{2}{\omega_1^2 W}, \quad W = \eta\xi, \quad A_0 = A - W, \tag{A11}$$

$$A = \frac{\omega_1}{K^2}\eta\xi[\omega_1(1-\eta) + (1+\eta)E(\tilde{\Delta}) + \eta\xi], \tag{A12}$$

$$B = \frac{2\omega_1 - \xi}{K^2}\xi\left\{\tilde{\Delta}^2 - \frac{\omega_1}{K^2}[(1-\eta)E(\tilde{\Delta}) - \eta\xi]\right\}. \tag{A13}$$

The significance of the variables is found in the main text: ξ and η are defined in Eq. (8). For K and $\tilde{\Delta}$, we use Eqs. (9) and (52), respectively. The behavior in the ER limit is simply

$$C \to W, \quad K \to \omega_1(1-\eta), \quad A \to \frac{\eta\xi}{1-\eta},$$

$$A_0 \to \frac{\eta^2\xi}{1-\eta}, \quad B \to 0 \tag{A14}$$

and leads to the result (69) in Sec. IV.

[1] P. M. Bergstrom, Jr. and R. H. Pratt, Radiat. Phys. Chem. **50**, 3 (1997).
[2] P. M. Bergstrom, Jr., T. Surić, K. Pisk, and R. H. Pratt, Phys. Rev. A **48**, 1134 (1993).
[3] T. Suric, P. M. Bergstrom, Jr., K. Pisk, and R. H. Pratt, Phys. Rev. Lett. **67**, 189 (1991).
[4] Z. Kaliman, T. Suric, K. Pisk, and R. H. Pratt, Phys. Rev. A **57**, 2683 (1998).
[5] L. LaJohn (private communication).
[6] V. Florescu and M. Gavrila, Phys. Rev. A **68**, 052709 (2003).
[7] V. Florescu and M. Gavrila, Rom. J. Phys. **48**, 639 (2003).
[8] P. Eisenberger and P. M. Platzman, Phys. Rev. A **2**, 415 (1970).
[9] R. Ribberfors, Phys. Rev. B **12**, 2067 (1975); **12**, 3136 (1975).
[10] R. H. Pratt *et al.*, Nucl. Instrum. Methods Phys. Res. B **261**, 175 (2007).
[11] P. Eisenberger and W. A. Reed, Phys. Rev. B **9**, 3237 (1974).
[12] R. H. Pratt, Phys. Rev. **117**, 1017 (1960).
[13] V. Florescu and M. Gavrila, Phys. Rev. A **14**, 211 (1976).
[14] J. M. Jauch and F. Rohrlich, *The Theory of Photons and Electrons* (Springer-Verlag, New York, 1976).
[15] When the quantized radiation field corresponds to one photon in the volume V, which is the case in deriving Eq. (25), the incident photon flux is c/V, which becomes $1/V$ in the units we use.
[16] V. Florescu and M. Gavrila, Radiat. Phys. Chem. **59**, 127 (2000).
[17] In fact, the reference systems S1 and S2 are in correspondence with those used by Ribberfors. Only the role of the incident electron in his case is played by the final electron in our case.
[18] L. LaJohn (unpublished).
[19] R. H. Pratt, L. A. LaJohn, V. Florescu, T. Suric, B. K. Chatterjee, and S. C. Roy, Radiat. Phys. Chem. (in press).